Report No. 176 / UILU ENG-97-4040

Modelling Variability in Vehicle Service Loading Histories

by

Kyung Hyun Park

B.S., University of Illinois at Urbana-Champaign, 1995

THESIS

Submitted in partial fulfillment of the requirements
for the degree of Master of Science in Mechanical Engineering
in the Graduate College of the
University of Illinois at Urbana-Champaign, 1997

Urbana, Illinois

ABSTRACT

Though multiple service loading histories may have the same general character for any given route, the magnitudes encountered in each history will vary from driver to driver. This variability in loading histories will be a function of the driving styles of the individual drivers, which in themselves have a significant level of variability. As the load history from any one driver will be variable and not a simple linear scaling of the history of any other driver, a simple linear scaling of any one history will not characterize the variability of usage over a wide range of service conditions. In this thesis, the effect on fatigue of the variation of service loads produced by different drivers operating a vehicle over a constant route will be presented. This will be accomplished through a statistical technique of measuring and extrapolating cumulative exceedance diagrams to quantify the distribution of loading histories. Necessary in this analysis is the fitting of a single three parameter Wiebull curve to the exceedance diagram. Also discussed is an automated procedure to perform such a fit. Monte Carlo simulations along with the local stress strain approach will be used to simulate a distribution for the varying service conditions imposed by the different drivers. These varying service conditions are the result of a novel approach in which loading histories were obtained through the use of a Four-Wheel Drive All Terrain Vehicle.

ACKNOWLEDGEMENTS

This thesis and the accompanying research activities were sponsored by the Ford Motor Company of Dearborn, Michigan. Much gracious assistance was also provided by the SoMat Corporation of Urbana, Illinois.

The author wishes to thank Dr. Darrell F. Socie, his graduate advisor, for the freedom to work independently and the patience and guidance along the course of this project.

Most importantly, the author's parents, Sang Jung and Sun Ai Park, are much thanked for their support and guidance.

TABLE OF CONTENTS

1. INTRODUCTION

1.1 Concerns in Design

In the face of intensifying consumer demands, regulatory requirements and marketplace competition, the resultant increasing requirements and constraints on costs, performance and durability have forced vehicle manufacturers to push the limits of almost every concept and element behind vehicle design. This is inclusive of concerns in structural elements and other load bearing components. Especially true is the need to ensure that such components will have sufficient durability in the face of the loading demands that they will encounter in service. However, with the continued pushing of the envelope, new methods of analyzing these loading demands have become necessary. Traditional design procedures called for a component of a given strength (determined by the mechanical properties of the material used in fabrication) to be exposed to a service load of a given stress value. However, it should be noted that materials fatigue is not a static process but a random and dynamic one. As seen in Figure 1, due to the random nature of vehicle service loading events, these events are variable and have a distribution about a mean value. Both the mean value and the variability will depend upon the service conditions of the component. Accompanying the loading variability in Figure 1 is the variable nature of the mechanical properties of the materials used in fabrication also with a distribution about a mean value. An overall safety factor is determined between the means of service loading and component strength distributions.

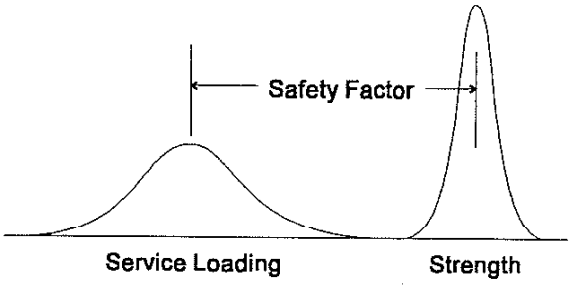

Figure 1, Loading Distribution Schematic

Generally, the distributions in the service loading events will be of a greater variability than the distributions of the material mechanical property values. In the analysis of loading histories, often the range-mean rainflow matrix histogram such as the one in Figure 2 is used. Such histograms provide a manner to more easily visualize the relationship between loading events and the number of events than typical time history plots. However, they are also more difficult to characterize by simple parametric distribution functions.

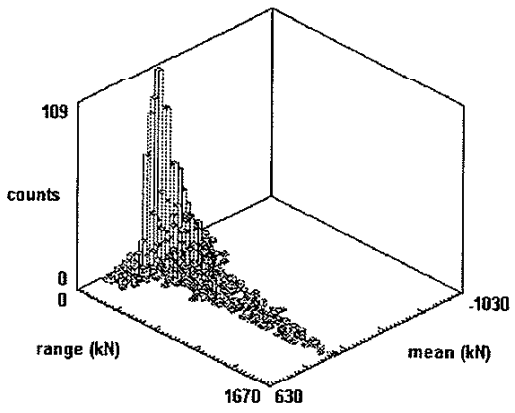

Figure 2, Rainflow Histogram

Utilizing the efforts of Socie and Park [1], an effort will be undertaken in this thesis to characterize the variability in service histories that are the result of variations in driving styles. This will be done by analyzing the differences in vehicle loading histories that are noted between different drivers while operating an instrumented vehicle over a constant test track.

1.2. Cumulative Exceedance Diagrams

In the analysis of multiple service histories, it can quickly be discerned that there is no simple relationship between any two service histories of any two different drivers. Although the two may pass over the same route, a simple linear scaling of the loading history of one will not appropriately represent the history of the other.

One method of analytical description of service loading histories is in the form of the Cumulative Exceedance Diagram. As noted in Socie in [2], the exceedance diagram such as the one shown in Figure 3 consists of rainflow counted ranges in the vertical axis and the cumulative number of cycles in the horizontal axis (typically plotted on a logarithmic scale). One advantage inherent in the simple exceedance diagram is that it can be represented by a Weibull curve with only three parameters. These parameters are the maximum strain, ε_{max}, maximum number of cycles in the service loading history, N_{max}, and a curve shape parameter, k where k is the Weibull slope. Also shown in Figure 3, a k-value of greater than unity yields a convex curve while a k-value less than unity yields a concave curve.

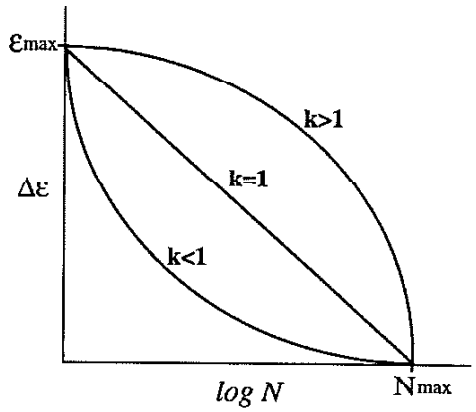

Figure 3, Schematic of Exceedance Diagram

Weibull distributions are often used to describe and extrapolate exceedance style data. The number of cycles at any given strain amplitude $N(\varepsilon_i)$ from a three parameter Weibull curve can be computed from the Weibull distribution function of Equation 1.

$$N(\Delta\varepsilon_i) = N(\Delta\varepsilon_{i-1}) - N_{max}\exp\left(-\left(\frac{\varepsilon_i}{\varepsilon_{max}}\right)^k \ln(N_{max})\right) \quad \text{.....(1}$$

)

The variables ε_{max}, N_{max} and k can be fit to any given set of exceedance data to yield a best fit Weibull curve to characterize that particular set of data.

2. PROCEDURE

2.1. General Requirements

For this effort, to analyze the variations in driving styles on vehicle service loading histories, a vehicle, a test track and an entourage of drivers was needed. For the sake of simplicity, a Four Wheel Drive All Terrain Vehicle was chosen as the vehicle. The use of a full sized passenger vehicle would have necessitated a full size test track of which there was no such availability. The costs associated with the construction of such a full-sized track would have also been prohibitive. An advantage of the ATV from the standpoint of the selection of drivers was the fact that the ATV selected was a relatively easy vehicle to operate, requiring minimal training to use and was fun to drive. To compliment the ATV, a test track over which to drive the ATV was required. An established test track was preferred as just merely driving the ATV over grass fields and mud patches would not have yielded consistent or repeatable results. For drivers, a general request was passed among students at the University of Illinois at Urbana campus. In all, 19 student drivers of varying driving skill levels volunteered their time and services to operate the ATV. Driver appointments were scheduled and the volunteer drivers were trained and given safety gear and control of the vehicle for their test drives. Actual testing occurred during the months of October through December of 1996.

2.2 Vehicle Description

As noted earlier, the vehicle of choice was a Four Wheel Drive All Terrain Vehicle. In particular, the ATV used was a 1995 year-model 300cc Honda FourTrax, as shown in Figure 4.

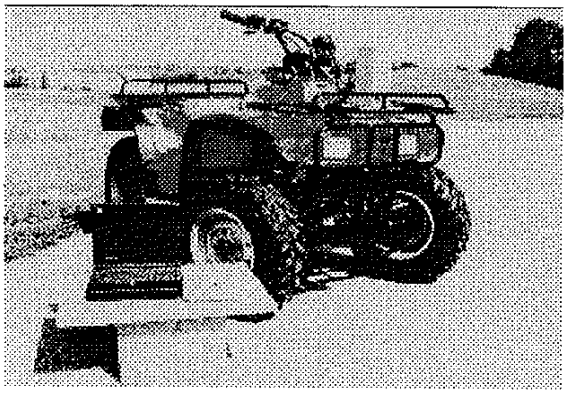

Figure 4, All Terrain Vehicle

Of particular interest regarding this ATV was the suspension system as seen in the schematic of Figure 5. The system in question was comprised of a fully independent setup in front and a live axle in the rear. A double wishbone design, the front suspension consisted of a pair of unequal length double control arms (upper and lower) with a coil spring and a shock absorber suspending each of the two wheels. In the rear of the vehicle was a suspension consisting of a live axle mounted to centrally-mounted trailing arms. Both trailing arms and rear wheels as well as the live axle were suspended by a single

shock absorber and coil spring. The similarity of the front suspension geometry to those found on passenger vehicles (the unequal length double wishbone design is in widespread use throughout the automotive industry in both front and rear suspension applications) lent the ATV well to simulating passenger vehicle loading characteristics.

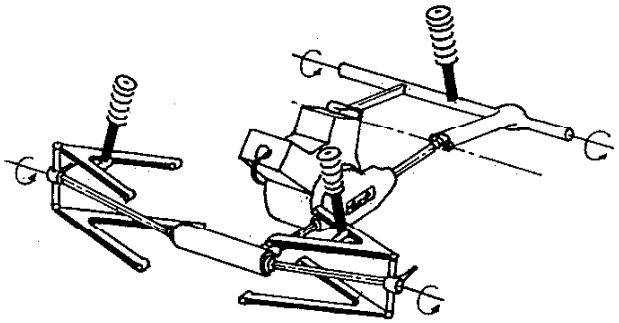

Figure 5, ATV Suspension and Powertrain Schematic

2.3 Instrumentation Description

Given the geometric similarity of the ATV front suspension to that found on a passenger vehicle, it was desired to take advantage of this similarity by measuring the loads sustained on the ATV front suspension to model passenger vehicle loading. This was facilitated through the instrumentation of various suspension components on the ATV.

Located on the front suspensions arms were two ball joints per side on the spindle. Being a double wishbone configuration, there was one ball joint on the upper arm and one on the lower arm, each ball joint connecting the respective suspension arm to the spindle.

The top ball joint on each side was equipped with strain gauges in three directions (fore-aft, lateral and vertical) and the bottom in two directions (fore-aft, lateral). Mounting of the ball joints was done in the configuration illustrated in Figure 6. These instrumented ball joints measured the loads in each of the respective directions applied to the suspension components in the course of operation.

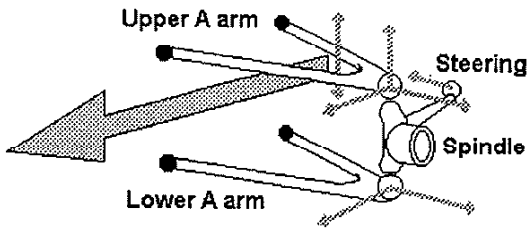

Figure 6, Front Suspension Geometry and Instrumentation Schematic.

A pair of linear displacement transducers (Figure 7), one on each side of the vehicle, were mounted to measure the vertical deflection (or wheel travel) of each of the two front wheels. The steering angle was measured via a rotary potentiometer spring mounted to the steering shaft. Mounting the potentiometer to the steering shaft was chosen as each of the two front wheels cut a different angle in turns due to the geometry of the steering system. This is due to a shared characteristic between this ATV and passenger vehicles known as the Ackerman angle. As the final channel, the measurement of vehicle speed was accomplished through the use of a pulse transducer mounted to the transmission final drive calibrated with respect to the vehicle speedometer.

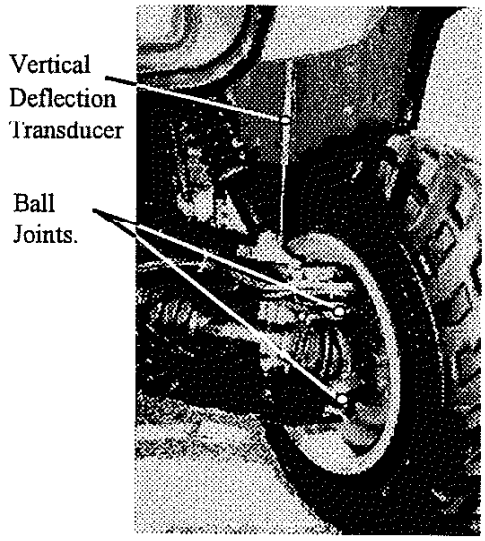

Figure 7, Front Suspension Detail

Data collection was handled by a modular 2100 series data acquisition field computer from the SoMat Corporation of Urbana, Illinois. This data collection unit consisted of a processor, memory and 14 separate signal conditioning modules. There was one channel module for each of the 14 channels of data (10 strain channels, one pulse channel and three analog channels). Power for the field computer was provided by the 12 volt DC electrical supply bus of the ATV. The field computer unit was located on the forward luggage rack of the ATV, in close proximity to the instrumentation connected to it. After each drive, the data collected during the drive was downloaded from the field computer to a laptop computer equipped with SoMat TCS for MS Windows® data acquisition software (Version 1).

A total of 14 channels in the configuration listed in Table 1 made up the instrumentation for the ATV. The first five channels numerically represented the five strain channels on the two ball joints on the left side of the vehicle. The final five represent the equivalent channels on the opposite side. The Input column denotes the input type used for each channel into the SoMat 2100 field computer.

Table 1, Instrumentation Data Channels

Channel No.	Channel Name	Channel Location	Channel Type	Input
Channel 1	Left Top BJ Lateral	LT Ball Joint	Strain Guage	Strain
Channel 2	Left Top BJ Fore Aft	LT Ball Joint	Strain Guage	Strain
Channel 3	Left Top BJ Vertical	LT Ball Joint	Strain Guage	Strain
Channel 4	Left Bottom BJ Lateral	LB Ball Joint	Strain Guage	Strain
Channel 5	Left Bottom BJ For Aft	LB Ball Joint	Strain Guage	Strain
Channel 6	Speed	Trans. Final Drive	Pulse Transducer	Pulse
Channel 7	Left Vertical Disp.	Left Wheel Well	Linear Transducer	Analog
Channel 8	Right Vertical Disp.	Right Wheel Well	Linear Transducer	Analog
Channel 9	Steering Angle	Steering Shaft	Rotary Pot.	Analog
Channel 10	Right Top BJ Lateral	RT Ball Joint	Strain Guage	Strain
Channel 11	Right Top BJ Fore Aft	RT Ball Joint	Strain Guage	Strain
Channel 12	Right Top BJ Vertical	RT Ball Joint	Strain Guage	Strain
Channel 13	Right Bottom BJ Lateral	RB Ball Joint	Strain Guage	Strain
Channel 14	Right Bottom BJ For Aft	RB Ball Joint	Strain Guage	Strain

2.4 Test Track Description

As a requirement to generate service loading data with the ATV, a driving course over which to drive the vehicle was needed. One option as a driving course was in driving the vehicle over a random set of terrain (grass fields, mud patches, nature trails, etc.). However, as this sort of driving would have been uncontrolled and unrepeatable due to the random selection of the terrain driven over, so also would the service loading data

collected by such driving. Efforts to contain such random course selection by repeatedly driving over the same section of soft terrain would eventually have resulted in the degradation of that driving surface. Such a degradation would have changed the characteristics of the terrain surface itself and, thus, changed the nature of the service loading data collected. Given all factors, the determination was in the construction of an established test track. Such a track would ensure repeatability in its ability to be driven over repeatedly and generate consistent data with each pass.

For the sake of simplicity and portability, an existing pavement structure was used for the base of the test track with the load event generators being in the form of a set of portable track modules. The track modules used were constructed of green-treated (i.e. weather-resistant) lumber and ¼ inch thick 4'x8' plywood sheets.

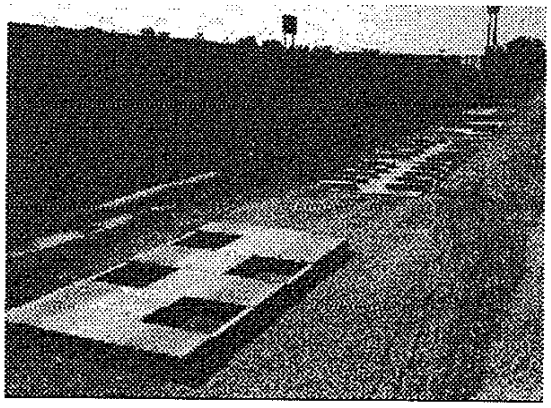

Figure 8, View of Test Track.

The final track configuration consisted of seven wooden track modules of four different module designs. These modules were located on an abandoned gravel frontage road as depicted in Figure 8. As noted in Figure 9, the basis of the data collected was from lining the modules in a single row and making repeated passes over the modules with the ATV. By driving the vehicle over the track in both directions, each side of the vehicle encountered both sides of the test track. With the definition of a single pass over the track as being a drive down the full length of the track modules one time, a total of 10 passes over the track were made by each driver for each data set collected (five passes in each of two directions).

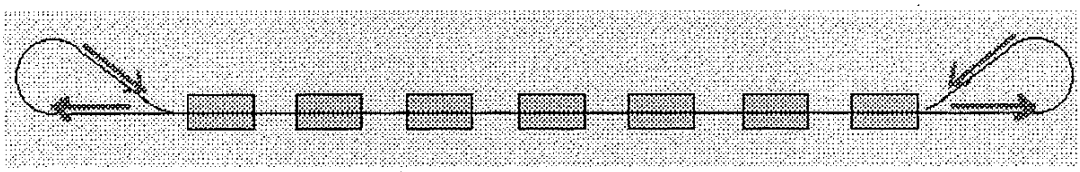

Figure 9, Pattern of Passes over Test Track

The first of the four track module designs was the Curb module (Figure 10). This module consisted of three equidistant 4.5-inch tall blocks, two half width and one full width mounted to a 4'x 8' plywood sheet. These blocks were composed of a single 2"x 4" wood stud (1.5"x 3.5" nominal with the smaller dimension being the height) affixed atop a pair of 2"x 6" studs (also each 1.5" in height). An offset pattern of the blocks had the vehicle see two events per side per pass. One module of this type was placed in the test track.

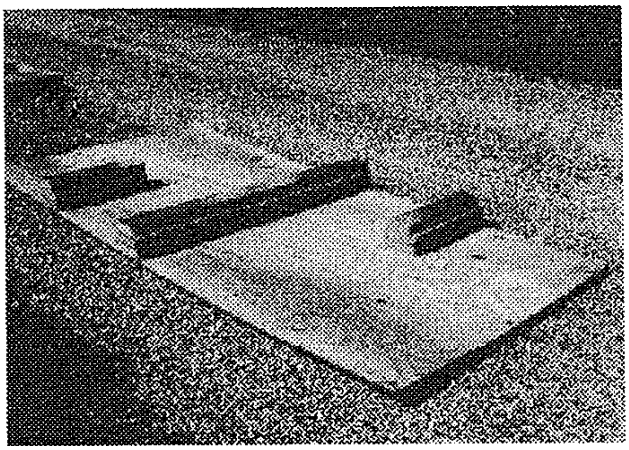

Figure 10, Curb Module

Alongside the curb module was the second module type, the ripple module. This module consisted of ten equidistant blocks each of a three inch height set in a staggered fashion. Similar to the curb module, the blocks were fashioned of a single 2"x 4" stud (1.5 inch height) affixed atop a single 2"x 6" stud (also of 1.5" height). With this module, the vehicle saw five events per side per pass over each module. Two ripple modules were installed in the test track as seen in Figure 11.

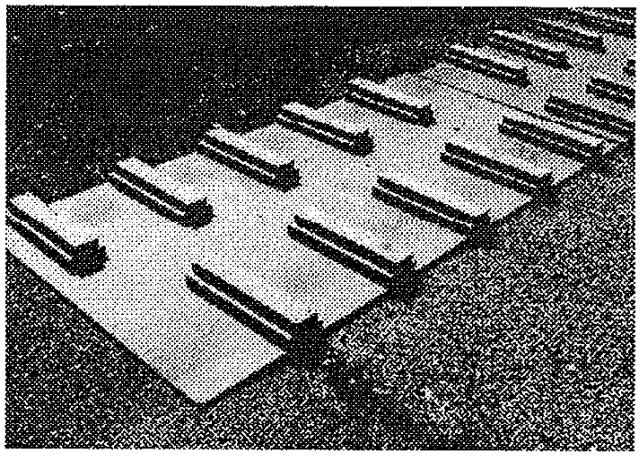

Figure 11, Ripple Module.

The third module type as seen in Figure 12 was the pothole module. As implied by the name, this module had four "potholes" cut into it. Each hole was an eighteen inch square cut into a 4'x 8' sheet with the sheet supported on top of 2"x 4"s (with the larger dimension being the height, giving a 3.5 inch nominal depth for each hole). Internal reinforcements in the module's hollow interior core were supplied by a set of additional 2x4's to ensure that the module would not flex and distort under the weight of the ATV. The four holes were set in a staggered fashion so that the vehicle would see two events per side per pass over each of the two such modules in the track.

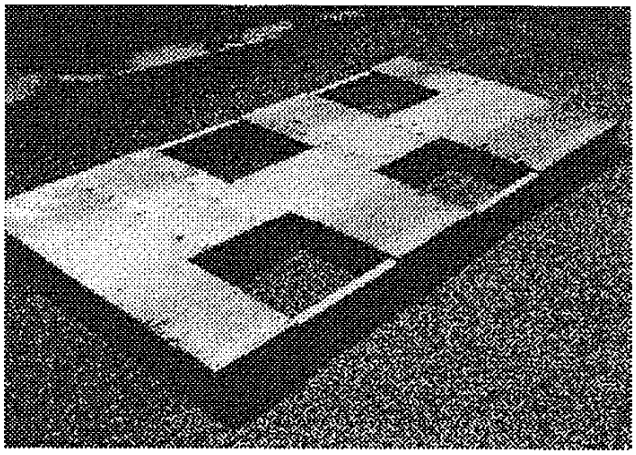

Figure 12, Pothole Module.

The fourth module type used was the tarstrip module. This module consisted of five one and a half inch nominal tall studs (2"x 4"s with the smaller dimension as the height) set at two foot intervals. The 2" x 4" studs were affixed longitudinally by a pair of 2"x 6" studs as seen in the schematic of Figure 13. Over the track, five events per side per pass were encountered by the vehicle over each of the two such modules in the track.

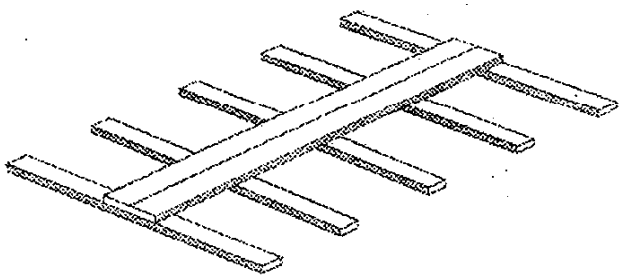

Figure 13, Tarstrip Module Schematic

2.5 Volunteer Drivers.

To obtain the needed variations in driving styles required for analysis, a small entourage of drivers was assembled to drive the ATV. Though all the volunteer drivers obtained were either students or recent graduates from the student body at the University of Illinois, exhibited was a fair level of variability within this sample pool of drivers in almost every measure of driving skill variation. A total of 19 volunteer drivers were retained. On the date of their driving appointment, each driver was asked to fill an evaluation form. The results of this form are listed in Table 2. The questions listed in the form included basic physical data such as gender information, weight and height. Another class of information sought was in terms of driving experience and violations information. In this sense, each driver was asked how many years of licensed driving experience each had with a passenger vehicle. The values ranged from 13 years down to as little as 1 week. Listed within parenthesis next to the experience with passenger vehicles was each driver's experience with motorcycles and ATV's, as applicable. Each driver was also queried regarding the number of traffic citations and at-fault vehicle accidents each was involved in within the previous five years. Another class of information sought was in self-ratings. Each driver was asked to rate themselves relative to the general public in terms of their driving ability and driving aggressiveness. As opposed to the other categories of questions which were objective in nature, these two questions were subjective.

Table 2, Driving Skills Survey of Volunteer Drivers.

	Gender	Weight	Driving Experience		Tickets	Accidents	Driving Ability	Aggressiveness
Driver 1	M	195	8yrs	(12yrs)	0	0	++	+
Driver 2	M	185	6yrs		0	0	+	0
Driver 3	M	135	13yrs		2	1	+	0
Driver 4	M	165	2yrs	(3yrs)	0	0	+	-
Driver 5	M	120	9yrs		0	0	+	0
Driver 6	M	225	5yrs		0	0	+	+
Driver 7	M	140	2yrs		0	1	0	--
Driver 8	M	165	5yrs	(5yrs)	3	1	+	+
Driver 9	M	195	5yrs	(12yrs)	0	0	+	--
Driver 10	M	150	5yrs	(1yr)	0	0	+	0
Driver 11	F	130	3yrs		0	0	+	0
Driver 12	M	220	9yrs		2	1	0	0
Driver 13	M	145	6yrs		0	0	+	0
Driver 14	F	105	1 week		0	0	0	-
Driver 15	F	100	5yrs		1	0	0	+
Driver 16	M	140	6yrs	(8yrs)	6	0	+	+
Driver 17	M	200	6yrs		3	2	0	-
Driver 18	M	140	7yrs		0	0	0	0
Driver 19	M	185	9yrs		0	0	+	0

Driving Ability (self evaluation)	++ much better than average, + better than average, 0 average, - worse than average, -- much worse than average	**Aggressiveness** (self evaluation)	++ much more aggressive than average + more aggressive than average, 0 average, - less aggressive than average, -- much less aggressive than average

3. RESULTS

3.1 Time History Format

Having equipped a vehicle with the necessary instrumentation and constructed a test track, the next step was in analyzing the data generated in the test drives. An example of the results from the combination of the instrumentation-equipped vehicle and the test track can be seen in the time history plot of Figure 14. Represented is a combination of the time histories of all 14 channels of data taken during the driving appointment of Driver 8. Observing the 14 time history plots, channel 9 is the steering angle. While driving, when the vehicle steering was centered and the vehicle aimed straight ahead (noted in the time history plot of channel 9 when the plot is dead center), the vehicle encountered a number of loading events as noted by the activity of channels 1-5 and 10-14. Shortly after the events subsided, the steering was turned (as noted by the steering angle plot wavering off center in either direction) and then straightened before the suspension loading events resumed. This is representative of the loading pattern of Figure 9. Though only representative of the data taken for only one of the 19 drivers, Figure 14 represents the general form of the data taken for all the drivers. Among the variations noted between the individual sets of data were such factors as time length (faster drivers completed the course in a shorter period of time than slower drivers), speed activity (some drivers varied their speeds more than others, usually upon approach to the track modules) and the severity of the loading events.

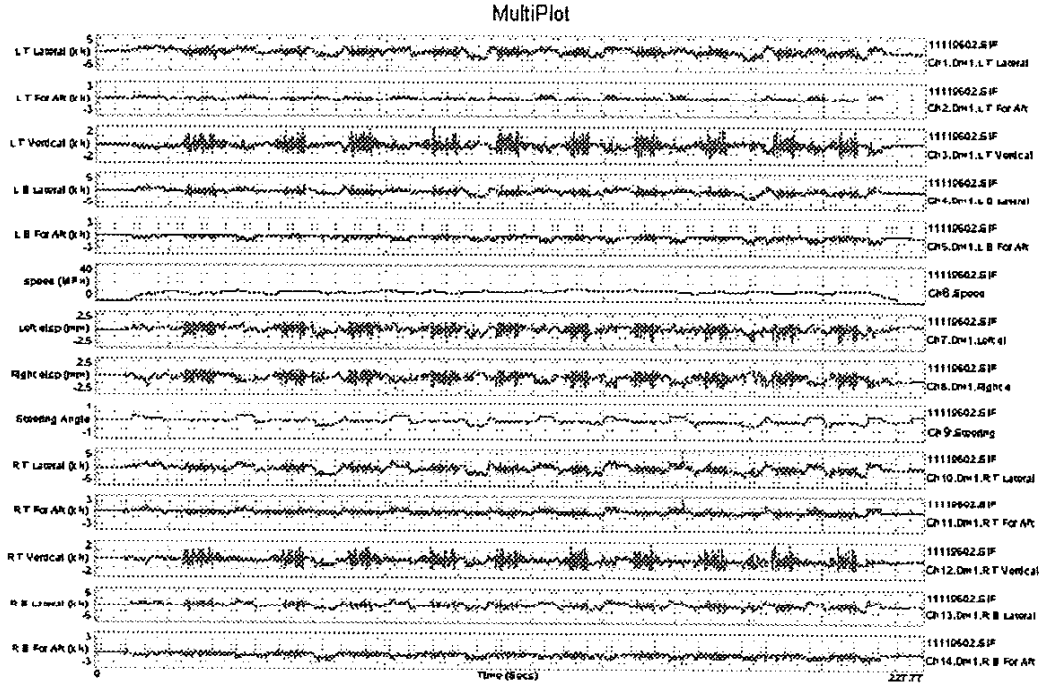

Figure 14, Time History Activity for One Driver

Demonstrating the variation between drivers is Figure 15. Two separate time histories between two different drivers (Drivers 1 and 8) for the same channel (Channel 3) are plotted. Variations between the two include time length and event magnitude. A simple scaling of either of the histories to characterize the other would not be appropriate.

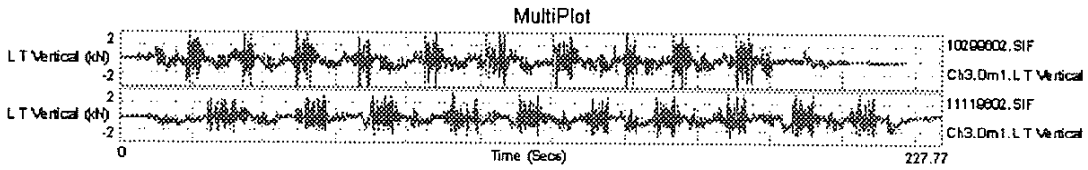

Figure 15, Comparison of Time Histories between Two Drivers

3.2 Cumulative Exceedance Diagram Format

With the objective to identify variances between different drivers and the effects that such variances have on vehicle service loading histories, a simple manner in which to visualize such variances was desired. The cumulative exceedance diagram described in [2] is one such solution. Figure 16 represents the familiar time history plot of a single data channel (Channel 3) for one driver (Driver 8) operating the ATV.

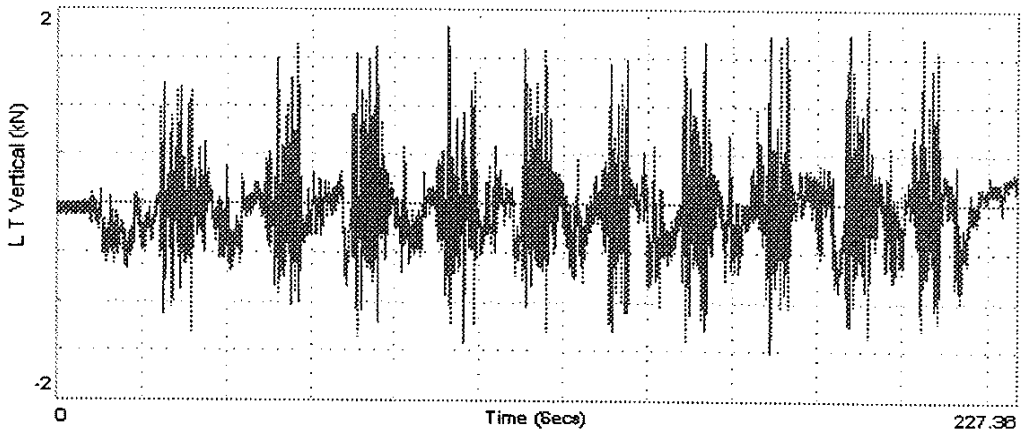

Figure 16, Time history plot (Chan. 3, Drvr. 8)

Converting the time history information into the cumulative exceedance format generates the plot of Figure 17.

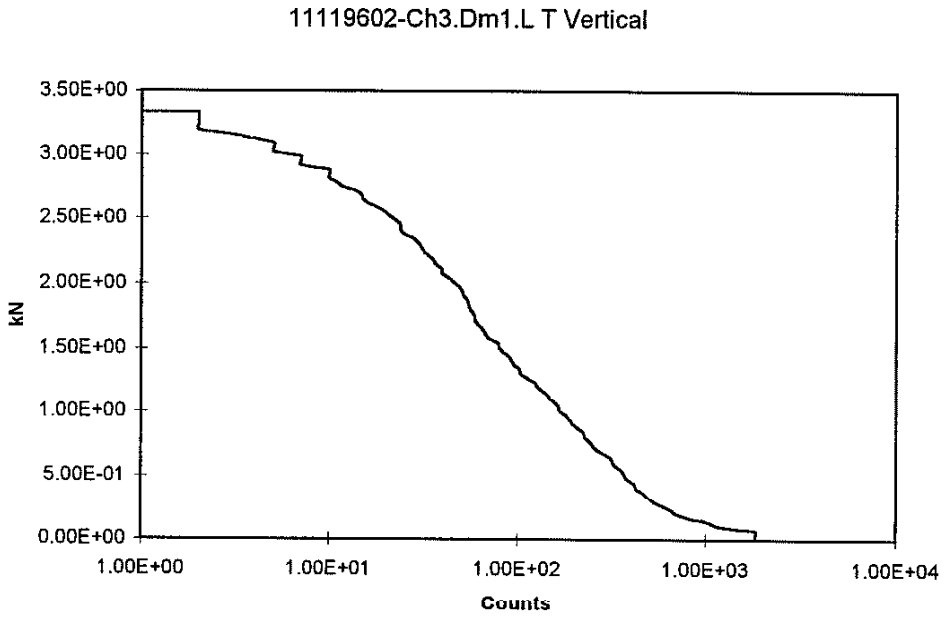

Figure 17, Cumulative Exceedance Diagram (Chan. 3, Drvr. 8)

Plotting the rainflow counted ranges in the vertical axis and the cumulative number of cycles in the horizontal axis generates an exceedance plot that gives a good idea of the proportion of the magnitude of loading events to the frequency of their occurrence. One tool available in the use of exceedance diagrams is in the direct comparison between multiple such diagrams of different service loading histories in exceedance form. In such a form, the differences between multiple service loading histories are easier to visualize and quantify. This can be seen in Figure 18 which represents the histories of all 19 drivers combined simultaneously into one exceedance plot for the same channel noted in Figures 16 and 17. A significant level of variance can be noted between the individual exceedance plots for the 19 drivers in this combined exceedance plot. An example of this variation

noted is in the maximum magnitude loading event achieved between the 19 drivers, a factor of approximately two being noted between the minimum and maximum such amplitude.

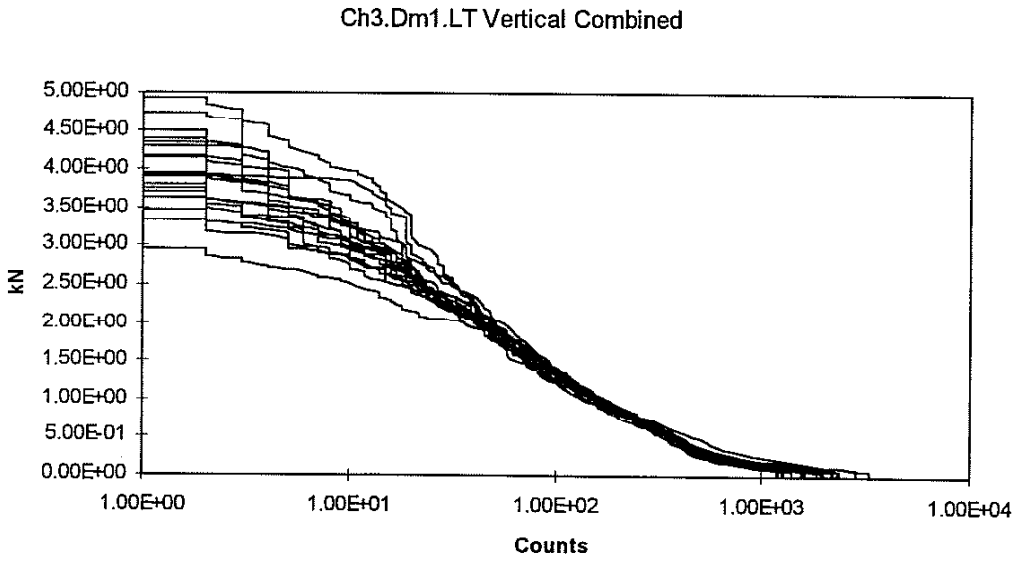

Figure 18, Combined Exceedance Diagram (Channel 3)

Given that Figure 18 is a representation of the service loading histories of the 19 drivers for only one of the 14 data channels, a similar process can be used to generate exceedance diagrams for the remaining 13 channels. However, when focusing specifically on the channels directly measuring values directly pertinent to fatigue calculations, only the 10 strain channels are involved. Noting that these 10 channels share symmetry about the vehicle center line, for the purpose of illustration, only five of the channels need be diagrammed. Choosing the five ball joint / strain gauge channels on the left side of the

vehicle (Channels 1-5) and adding the accompanying vertical displacement channel (Channel 7) for visual reference, the exceedance diagrams of the load histories for the 19 drivers for the six channels in question are plotted in Figure 19 a) through 19 f).

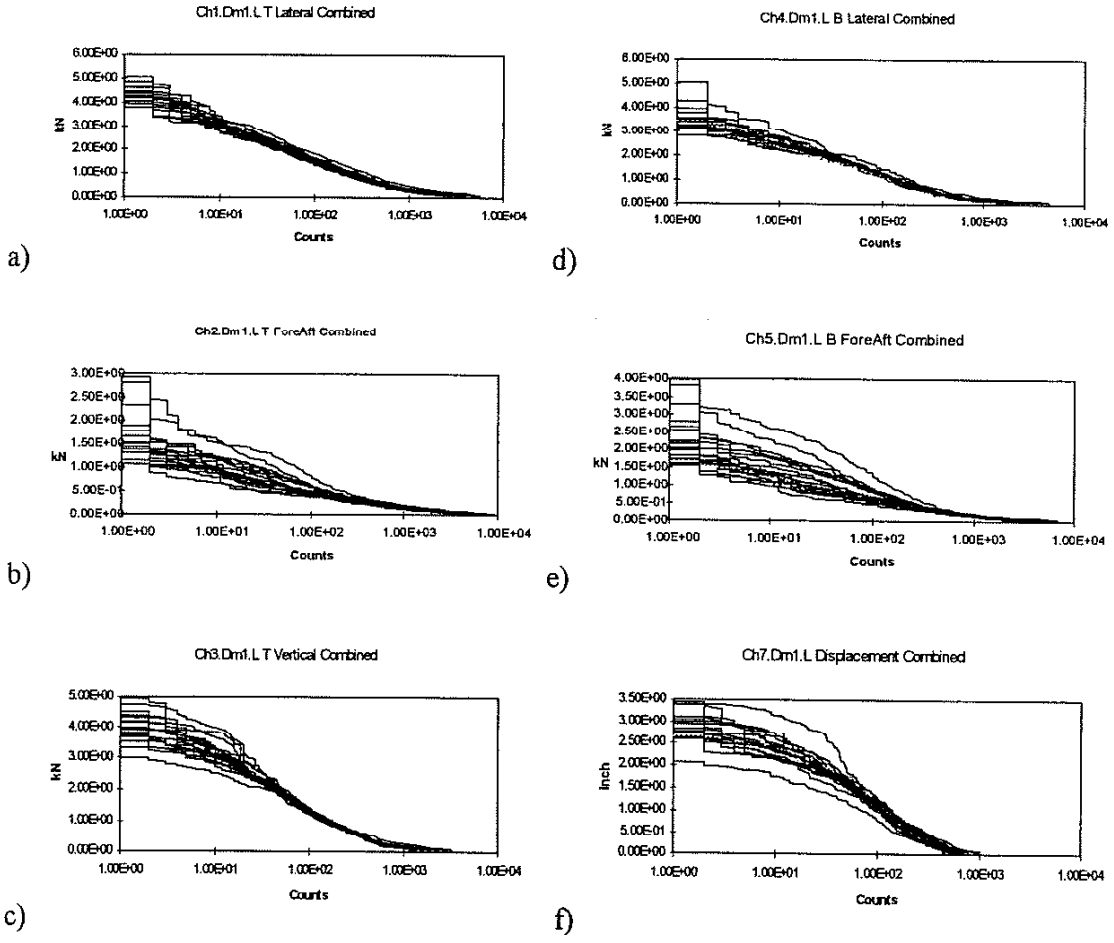

Figure 19, Exceedance Diagrams for Six Channels and 19 Drivers

As in Figure 18, significant levels of variation can be noted between the individual exceedance plots between the 19 drivers. This variation is evident in all six channel plots.

In terms of magnitudes, the channels dedicated to lateral forces revealed the least variation between drivers while the fore-aft channels revealed the most. Some variance is also observable from the standpoint of the number of higher amplitude loads seen, particularly in the vertical displacement channel (Channel 7). Given symmetry constraints, exceedance plots for the equivalent channels on the right side of the vehicle are similar.

3.3 Weibull Fitting of Cumulative Exceedance Diagrams

As noted previously, utilizing the Cumulative Exceedance Diagram format to display the service loading history data in exceedance form enables the use of a fitted three-parameter Weibull curve to characterize it. A Weibull curve that best fits the exceedance data represents a good model of that particular exceedance data set itself. However, necessary for analysis is a methodology of finding such a good fit curve. A reasonable fit curve can be obtained by "eyeballing" the curve, by iterating with different values of N_{max} and k (since ε_{max} is constrained by the exceedance curve, it is already known) until a visually appeasing curve is achieved. However, such "eyeballing" is inconsistent and time consuming. An automated fitting method is preferred for more consistent results.

In developing an automated curve fitting routine for the exceedance diagrams, a linear fitting routine can be used. Non-linear regression fitting, though possible, would involve extra complexity to what would otherwise be a relatively simple routine. To

linearize the exceedance data, the equation for the three parameter Weibull curve (Equation 1) is modified into a linear format,

$$N(\varepsilon_i) = N_{max}\exp\left(-\left(\frac{\varepsilon_i}{\varepsilon_{max}}\right)^k \ln(N_{max})\right),$$

$$\ln(N(\varepsilon_i)) = \ln(N_{max}) - \left(\left(\frac{\varepsilon_i}{\varepsilon_{max}}\right)^k \ln(N_{max})\right),$$

$$\ln(N(\varepsilon_i)) = \ln(N_{max})\left(1-\left(\frac{\varepsilon_i}{\varepsilon_{max}}\right)^k\right), \quad \text{.....(2)}$$

$$y = mx$$

where $y = \ln(N(\varepsilon_i))$, $m = \ln(N_{max})$ and $x = \left(1-\left(\frac{\varepsilon_i}{\varepsilon_{max}}\right)^k\right)$

Placing the entire range of exceedance data points for any given data set into the individual parameters for x and y yields a plot dependent upon the k parameter for the x-variable. Adjusting this k parameter until the best straight line with slope m = ln(Nmax) is obtained would determine the k parameter best suited for fitting the entire range of exceedance data. However, in fitting the exceedance data, it must be noted that fitting the entire range of exceedance data may not necessarily give the best fit Weibull curve. Indeed, it usually will not. As seen in Figure 20, this is due to the fact that exceedance diagrams often take on a two stage curve form, with a primary curve covering the higher magnitude, low cycle spectrum and a secondary curve covering the lower magnitude, high cycle spectrum. Depending on the nature of the specific exceedance data set, a single three

parameter Weibull curve usually will not adequately fit the entire spectrum of exceedance data. Therefore, a certain segment of the data spectrum should be identified as being of more importance in fitting.

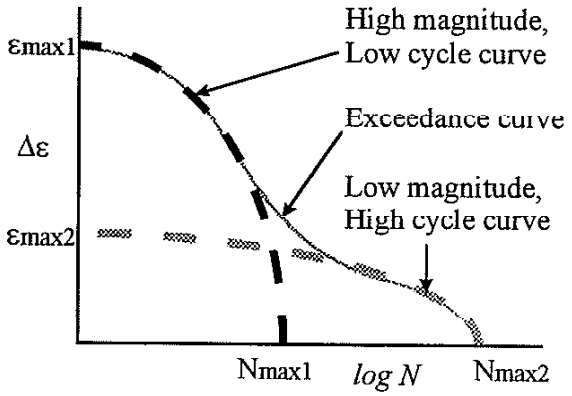

Figure 20, Schematic of Two Stage Nature of Exceedance Curves

Between the higher magnitude strain curve values and the lower magnitude strain curve values, the higher strain values will contribute significantly more to fatigue damage than the lower strain values. This can be visualized in the damage histogram of Figure 21 b) which is the damage histogram of the rainflow range-mean histogram of Figure 21 a). Though the majority of loading events described in rainflow histogram occur in the lower strain range region, the loading events responsible for the majority of the damage are the small number of higher loading events as seen in the damage histogram. Therefore, the important data segment for priority curve fitting is the higher magnitude, low cycle regime. Indeed, the lower strain values on the exceedance diagram can be ignored in the curve fit with negligible impact on the extrapolated fatigue lives.

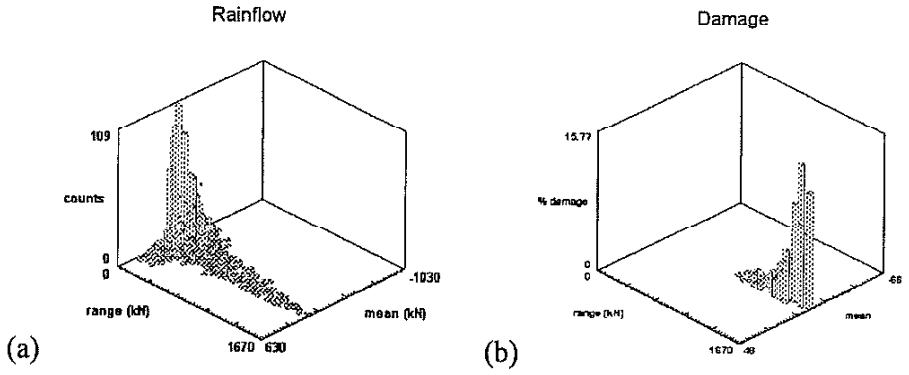

Figure 21, Rainflow Histogram (a) and Damage Histogram (b)

A high magnitude regime cut-off value in the exceedance data must be determined for use in fitting the higher magnitude Weibull curve. The manner in which this cut-off for the selection of which segment of the exceedance data should be fitted to and which should be ignored is through a selective slope fitting method. In this method, as outlined in Figure 22 a), the local slopes of various points along the exceedance curve are determined. The point at which the maximum slope on the curve occurs is also the point at which a properly fitting higher magnitude Weibull curve would likely begin to lose fit to, and diverge away from, the exceedance curve. It is at this point where the cut-off is established for Weibull fitting as seen in Figure 22 b). All points along the exceedance curve before the global maximum slope cut-off point are used in the fitting. All points after are ignored as such points would constitute the lower magnitude curve which is of lesser importance in determining fatigue damage.

Following the selection of a global maximum slope cut-off point, all data points preceding the cut-off are placed into the linearized Weibull equation of Equation 2). This

linearized equation contains the k parameter in the x-component. As seen in Figure 22 c), adjusting the k parameter in the x component will yield different shapes for the resulting linearized plot. The value of k which results in a best fit to a straight line of slope "m" is the k value for the Weibull plot. This best fit slope "m" is defined in Equation 4) and is equivalent to the "m" value noted in Equation 2).

$$\mathbf{error} = \varepsilon = \mathbf{mx'-y}$$

$$\sum \varepsilon^2 = \sum (\mathbf{mx} - \mathbf{y})^2, \quad \text{.....(3)}$$

$$\sum \varepsilon^2 = \sum (\mathbf{m}^2\mathbf{x}^2 - 2\mathbf{mxy} + \mathbf{y}^2)^2,$$

$$\sum \varepsilon^2 = \mathbf{m}^2 \sum \mathbf{x}^2 - 2\mathbf{m} \sum \mathbf{xy} + \sum \mathbf{y}^2,$$

$$\frac{\partial \sum \varepsilon^2}{\partial \mathbf{m}} = 2\mathbf{m} \sum \mathbf{x}^2 - 2 \sum \mathbf{xy} = \mathbf{0},$$

$$2\mathbf{m} \sum \mathbf{x}^2 = 2 \sum \mathbf{xy},$$

$$\ln(\mathbf{N}_{max}) = \mathbf{m} = \frac{\sum \mathbf{xy}}{\sum \mathbf{x}^2} \quad \text{.....(4)}$$

where $\sum \mathbf{xy} = \mathbf{x}_i * \mathbf{y}_i + \mathbf{x}_{i+1} * \mathbf{y}_{i+1} + \ldots\ldots + \mathbf{x}_n * \mathbf{y}_n$

$\sum \mathbf{x}^2 = (\mathbf{x}_i)^2 + (\mathbf{x}_{i+1})^2 + \ldots\ldots + (\mathbf{x}_n)^2$

The definition for this "best fit" to the straight line of slope m is given through an error summation function as noted in Equation 3). The error measured by this function is the difference in the y-values between the actual y-value from the data and the y value for the line at a corresponding x-point (x multiplied by the line slope, m). This summation

function is performed throughout the entire range of exceedance data values before the cut-off point. The value of k which yields the smallest error summation between the straight line and the curve is the k-value selected as the shape parameter for the Weibull curve as seen in Figure 22 d).

Knowing that fatigue damage is a function that varies between the fourth power to the tenth power of the applied strain, this fact can be used as a weighting function for the error summation process. Given that the higher magnitude events play a far more significant role in determining fatigue damage than the lower magnitude events, it is desired that these higher magnitude events be fitted more closely than the lower magnitude events. Though a fourth power function would give the least weighting to the larger load events and a tenth power function the most weight, a weighting function of the fourth power would assure a close fit of the Weibull curve in the high magnitude strain regime without sacrificing excessively the fit to moderate magnitude events. An additional factor in the weight function is the number of cycles that each magnitude event occurred. This factor assures a closer fit to larger events that occur most frequently. The result is a fit that is biased towards the most fatigue damage. The weight function utilized is the fourth power of the strain range value multiplied to the number of cycles that strain range value occurred multiplied to the corresponding exceedance curve point in the x and y parameters as seen in Equation 5).

$$\mathbf{error} = \mathbf{mx'} - \mathbf{y}$$

$$\sum \text{error}^2 = \sum (mx' - y)^2$$

$$\sim \text{Weight} * \sum (mx' - y) - N \Delta\varepsilon^4 \sum (mx' - y), \quad \text{.....(5)}$$

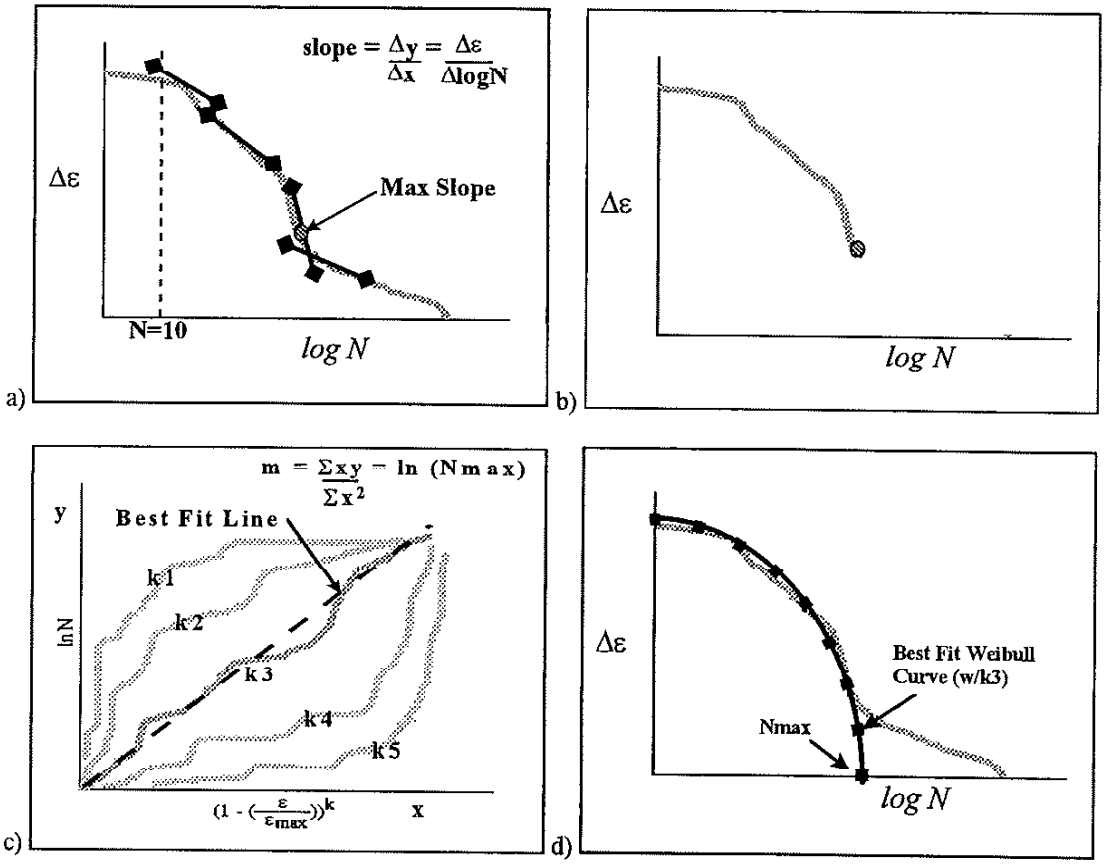

Figure 22, Schematic Procedure of Weibull / Exceedance Curve Fitting

One criterion established in the cut-off is in the fact that at the high magnitude, low cycle region of the exceedance curve, localized slope perturbations may occur duc to the random nature of the service loading history data. Such perturbations in the low cycle region may result in a locally high slope value for the exceedance curve in that region. If

such a localized high slope value were to exceed the global maximum slope value, it would then be used by the slope fitting routine to establish the cut-off point. Such a premature cut-off would be unacceptable as it would leave only a very minimal amount of exceedance data to fit a Weibull curve to (since the cut-off occurred so early). An early cut-off would also likely result in an improper overall fit of the exceedance data. Therefore, an acceptable minimum permissible cut-off point should be imposed, before which, the global cut-off would not occur regardless of high local slope values. In this analysis, the minimum cut-off was set at 10 cycles as seen in Figure 22 a).

Pursuit of the above procedures for the Weibull curve fitting of the exceedance diagrams will yield Weibull curves with a good level of fit to the exceedance data as seen in Figure 23 (Channel 3, Driver 11).

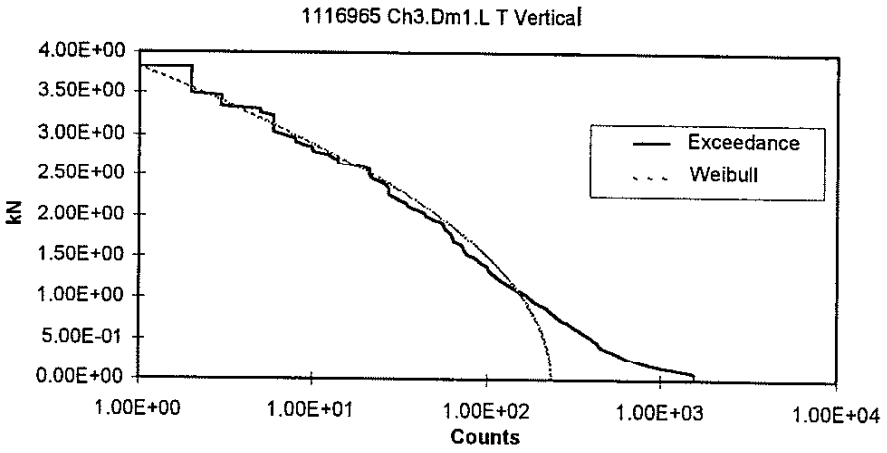

Figure 23, Weibull Fitting to Exceedance Data (Chan. 3, Drvr. 11)

3.4 Monte Carlo Analysis

Each of the three Weibull variables, ε_{max}, N_{max} and k can be treated as random variables in their own right. As random variables, each of the three will have their own statistical distributions. For the ten strain channels, a statistical distribution can be generated for the three parameters. This can be done by analyzing the variability of the parameters among the 19 drivers for each channel. Statistical manipulation of these distributions for the three parameters can produce a number of variable amplitude loading histories for each channel. Contained in Table 3 are the constants for the three parameters obtained from the Weibull curve fit to all 19 data sets for Channel 3.

Table 3, Results from Curve Fitting (Channel 3)

$\Delta\varepsilon_{max}$	Nmax	k
1173.75	63.396	4.05
1083.5	84.797	4.05
1075.75	269.943	1.65
1025.25	181.821	2.2
1035.203	266.170	1.7
985.125	117.965	2.8
901.48	350.433	2.15
797.05	193.518	3.55
970.7325	162.664	2.55
888.275	210.893	2.45
975.7225	75.656	4.2
902.475	211.337	2.3
1086.873	92.837	3.4
826.675	271.699	2.45
873.875	236.004	2.35
1206.035	882.618	0.9
901.4725	102.079	3.85
826.6825	197.262	3.85
718.0975	404.975	2.65

Table 4 presents the statistical distributions of the data in Table 3. Considering the limited sample size of 19, a LogNormal distribution was used in the accompanying analysis. Verification of the LogNormal distribution is provided by Figure 24 which is a LogNormal plot for $\Delta\varepsilon_{max}$.

Table 4, Distribution of Variables (Channel 3)

	$\Delta\varepsilon_{max}$	Nmax	k
Distribution	LogNormal	LogNormal	LogNormal
Mean	960	230	2.79
COV	0.13	0.79	0.33

$$\text{where COV} = \frac{\sigma_x}{\mu_x}$$

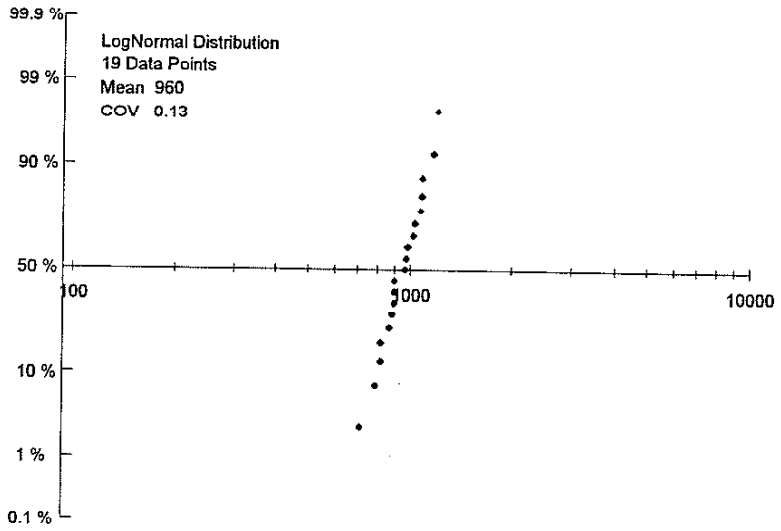

Figure 24, LogNormal Distribution of $\Delta\varepsilon_{max}$

Table 5 contains the correlation coefficients between the variables. A significant level of correlation exists between the k shape parameter and the N_{max} values. This correlation is understandable since, for a constant $\Delta\varepsilon_{max}$ value, a higher k value will generally accompany a lower N_{max} value in a Weibull fit. The correlation between the other variables is relatively weak.

Table 5, Correlation Between Variables (Channel 3)

	Δεmax	*Nmax*	*k*
Δεmax	1		
Nmax	0.0150	1	
k	0.0205	0.5340	1

Pursuing Equation 1, each of the variables in the equation can be replaced by a value based on the statistical distributions given in Table 4. With this statistical manipulation, any number of Weibull curves and, thus, service loading histories can be obtained. Complicated numerical methods are necessary to obtain a solution due to the complex statistical distributions associated with each variable. One simple but useful technique in this manner is the Monte Carlo method. In general methodology, a sample of each of the three variables is drawn at random from its distribution and a single deterministic loading history is generated. In the case of the Monte Carlo simulation, this analysis is performed by selecting a random number between 0 and 1. This random number is then transformed into a specific value for each input variable knowing the distribution function for the variable.

Employing the familiar Coffin-Manson strain-life equation of Equation 6, fatigue lives can be computed for each simulated service loading history. The relationship between strain amplitude and fatigue life is given by this equation. The strain life material property values for 980X steel used in these calculations are listed in Table 6 and are the same as those used in [2].

$$\left(\frac{\Delta\varepsilon_i}{2}\right) = \left(\frac{\sigma'_f}{E}\right)(2N_f)^b + \varepsilon'_f\,(2N_f)^c \quad \text{.....(6)}$$

Table 6, Material Properties for 980X

σ'f	Fatigue Strength Coefficient	1315 MPa
b	Fatigue Strength Exponent	-0.097
ε'f	Fatigue Ductility Coefficient	0.253
c	Fatigue Ductility Exponent	-0.556
e'f	Modulus of Elasticity	208 GPa
K'	Cyclic Strength Coefficient	1675 MPa
n'	Strain Hardening Exponent	-0.17

Demonstrating the viability of the Monte Carlo numerical analysis, results for 1000 Monte Carlo simulations for three selected strain channels are given in Figures 25 through 27. In each plot, the square symbols represent the fatigue estimates obtained from the analysis of the original 19 loading histories for each of the three illustrated channels. Listed within each plot is a distribution (mean and coefficient of variation) for each of the three Weibull variables used in the simulation.

The level of agreement between the life estimates from the 19 original loading histories and the 1000 simulated histories generated through the use of the Monte Carlo analysis are generally good.

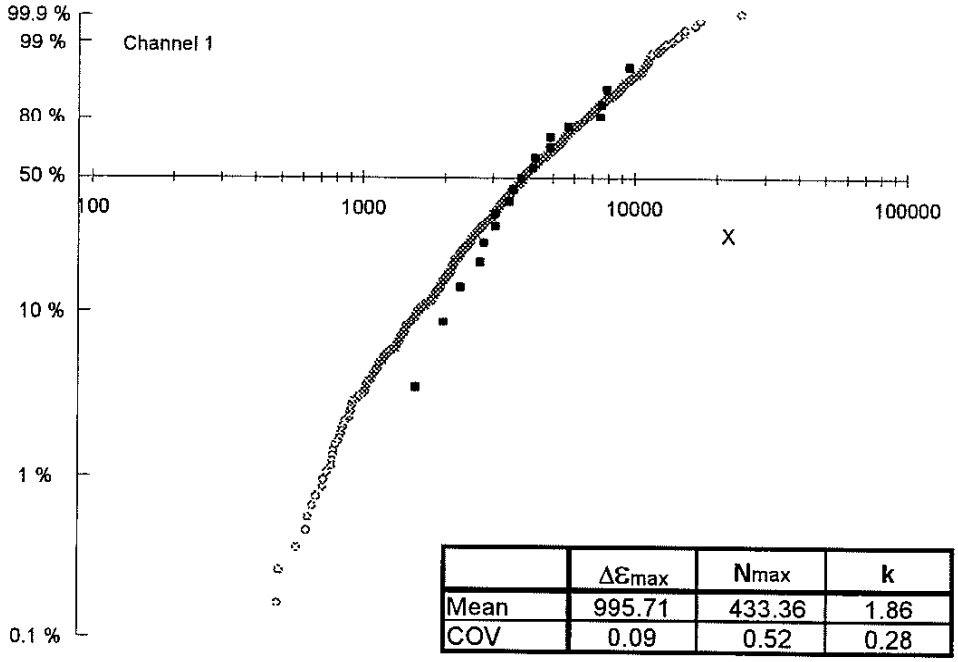

	$\Delta\varepsilon_{max}$	Nmax	k
Mean	995.71	433.36	1.86
COV	0.09	0.52	0.28

Figure 25, Simulation Results (Channel 1)

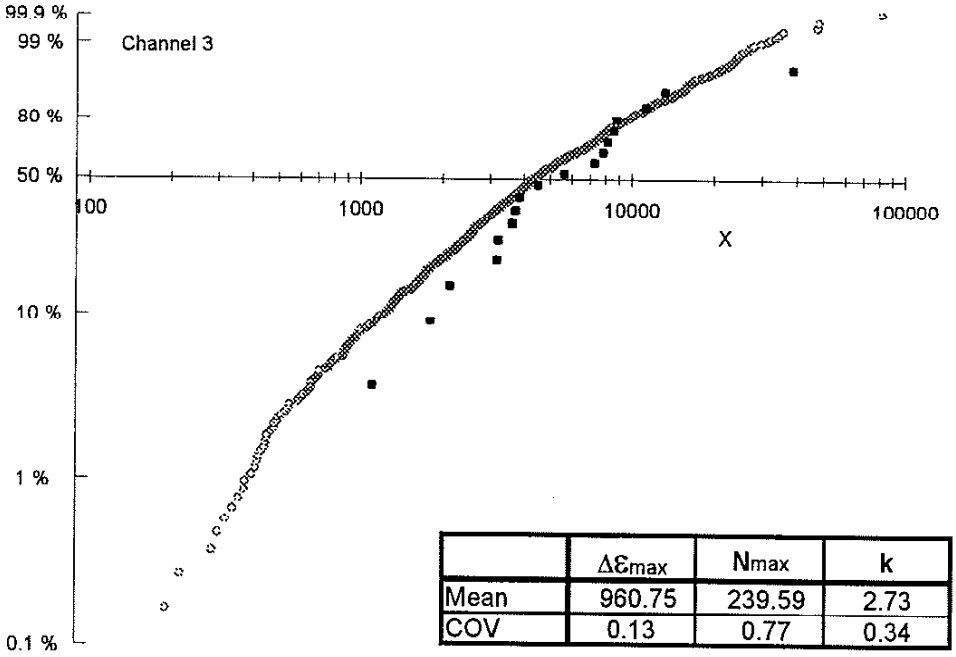

	$\Delta\varepsilon_{max}$	Nmax	k
Mean	960.75	239.59	2.73
COV	0.13	0.77	0.34

Figure 26, Simulation Results (Channel 3)

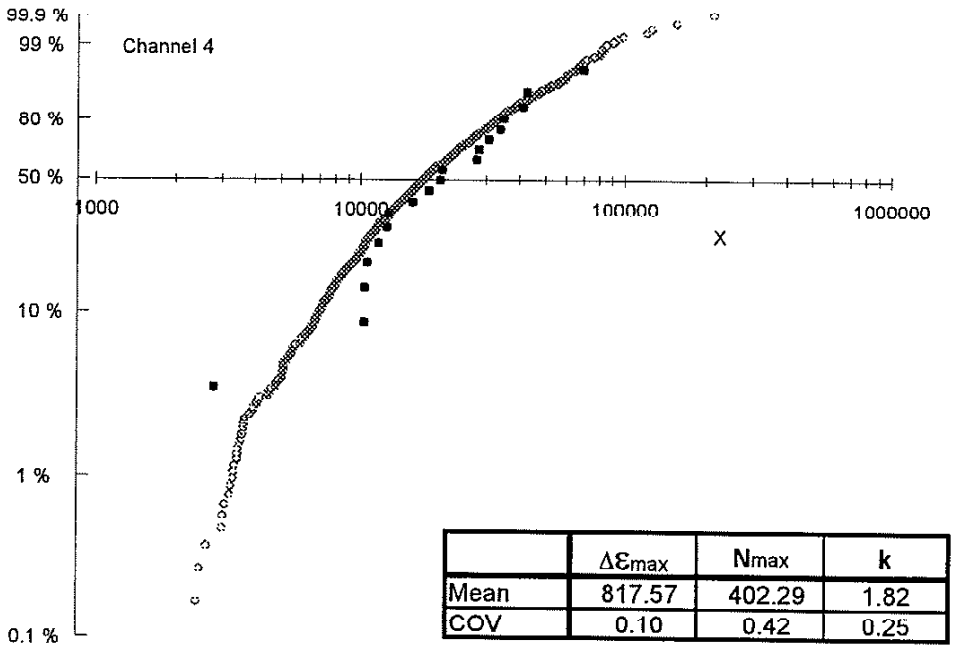

	$\Delta\varepsilon_{max}$	N_{max}	k
Mean	817.57	402.29	1.82
COV	0.10	0.42	0.25

Figure 27, Simulation Results (Channel 4)

Listed in Tables 7 to 9 are the correlation coefficients between the three Weibull variables and the life estimates generated by the simulations. In all cases, a high degree of correlation exists between the life estimates and the $\Delta\varepsilon_{max}$ values. This is to be expected given the strong relationship between imposed strains and cyclic life. This relationship is noted by the rainflow and damage histograms of Figures 21 a) and 21 b) as well as the Coffin-Manson strain-life equation of Equation 6. A more modest correlation is also seen between the life estimates and the k shape parameter. Again, this is understandable noting that a higher k parameter will make the Weibull curve more convex, increasing the number of higher magnitude cycles in the simulations. The result of an increase in the k-value and the accompanying increase in the number of higher magnitude cycles would be a reduction in expected fatigue lives. In all three cases, the relationship between the life estimates and the N_{max} values is relatively weak.

Table 7, Correlation Between Variables (Channel 1)

	Δεmax	*k*	*Nmax*	*Life*
Δεmax	1			
k	0.0008	1		
Nmax	0.0019	0.0011	1	
Life	0.5844	0.1832	0.0136	1

Table 8, Correlation Between Variables (Channel 3)

	Δεmax	*k*	*Nmax*	*Life*
Δεmax	1			
k	0.0008	1		
Nmax	0.0012	0.0006	1	
Life	0.4763	0.0895	0.0188	1

Table 9, Correlation Between Variables (Channel 4)

	Δεmax	*k*	*Nmax*	*Life*
Δεmax	1			
k	0.0009	1		
Nmax	0.0022	0.0013	1	
Life	0.4296	0.0801	0.0020	1

As seen from the analysis, the variations in the driving styles of the 19 volunteer drivers yields a significant level of variability from the standpoint of fatigue. Depending on the channel, this variability in fatigue lives of the original loading histories is from one to one and a half orders of magnitude from the lowest to highest values. Not surprisingly, between the 1000 simulated loading histories, this variability in fatigue estimates is slightly higher. The variability in this case ranges from two to three orders of magnitude.

With the original loading histories, the ability to generate an estimate of the reliability or estimate of more severe usage beyond the most severe history in the data set was limited. However, the statistical simulation model presented can easily generate such an estimate. As an example, referring to Figure 26 (Channel 3), an estimate of the 99.9% reliability can be made. Using the results from the Monte Carlo simulations, the 99.9% reliability case yields a fatigue life estimate one and a half orders of magnitude smaller than the mean life of 4.3×10^3 cycles. In Figure 28, a representation of a possible exceedance diagram of this most severe loading case is presented. The original 19 loading histories for Channel 3 are plotted for reference. It is interesting to note that both the maximum loading range and the number of higher amplitude loads of the 99.9% reliability case are increased. A linear scaling of any one of the original histories would not have produced this result. It should also be noted that any one of a number of possible combinations of the appropriate three Weibull parameters would also have yielded an identical result.

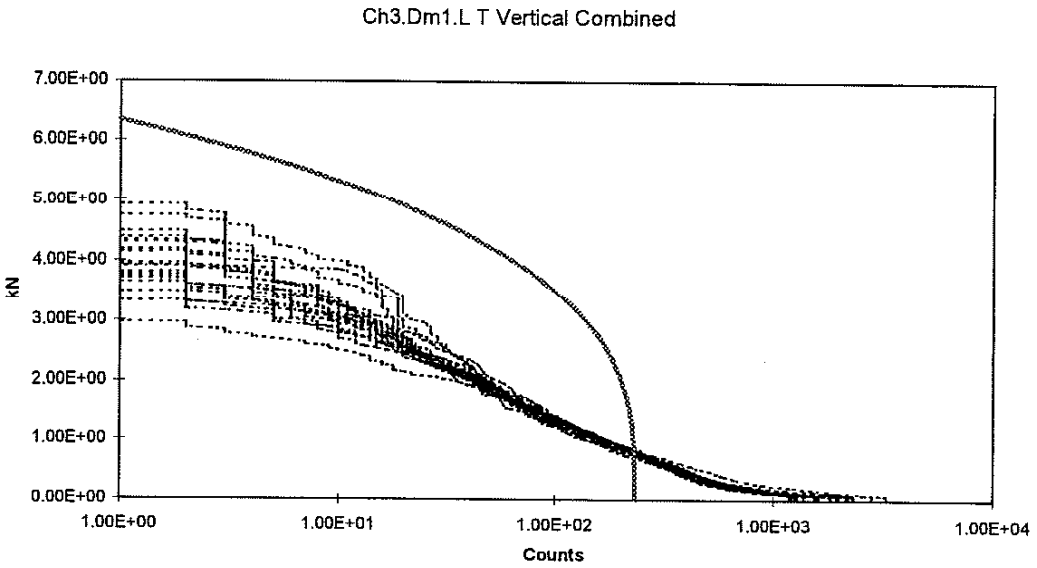

Figure 28, 99.9% Reliabilty Loading Simulation (Channel 3)

4. FUTURE RECOMMENDATIONS

The analysis performed in [2] made use of a two curve distribution to characterize both the high load curve and the lower load curve as illustrated in Figure 20. The data that

was obtained from the ATV, however, did not display as much of a two-curve tendency as that from [2]. Part of this difference can be attributed to the test track used for the ATV which emphasized larger loading events as opposed to smaller loading events. With fewer smaller load generating track modules, the resultant exceedance plots reflected fewer events of a smaller load nature. Correspondingly, there was a smaller tendency to have a secondary lower magnitude curve in the exceedance diagram. Certainly, fitting the larger load curve is certainly still of more importance than in fitting the smaller load curve from a fatigue standpoint. However, if the exceedance diagram in question contains a significant number of smaller to moderate sized events in a visually distinct lower magnitude curve, fitting this separate curve would be desirable for optimum accuracy in fitting. Utilizing the exceedance data after the maximum slope cut-off described along with the linearized Wiebull equation is one potential method in handling such a fitting. Unlike the larger load curve, however, the smaller curve does not have a distinct maximum strain range value to use as an anchor in the estimates of the other two parameters. As with the larger load curve, the maximum cycle count for the exceedance data, N_{max}, again may not serve appropriately as the N_{max} for the Weibull curve. An iterative fitting procedure would be needed to find a best fit value for all three parameters.

Noting the limited sample size of data sets for each of the channels of 19, a larger sample size would be desired. Statistically speaking, the minimum useful sample size is approximately 30. A higher sample size, of course, would be desired. Continuing data collection with additional drivers and using drivers from different sample populations (other than college students as with the current sample population) would yield a more

statistically useful distribution of data. Given that the Monte Carlo simulation method relies upon the data collected from the ATV as the basis of its simulations, a larger sample pool of drivers would also improve the accuracy of the Monte Carlo simulations.

It should also be noted that service loading histories are not the only source of variability in determining the durability of vehicle structural components. Other sources of variability include those in material properties and manufacturing concerns. Variability in materials properties can be a function of initial flaw sizes, material purity, alloying compound compositions, grain sizes among others. Variability in manufacturing can include variations in machining and die and mold dimensions. Simulation methods similar to the one presented here to analyze the variability in service loading histories can also be used to evaluate these sources of variability

5. CONCLUSIONS

The magnitudes encountered in multiple service loading histories will vary between any two drivers even if the two drivers traverse the same route. As any one loading history from any one driver is variable, it cannot be represented by a simple linear scaling of the history of any other driver. By the same token, the variability in the severity of usage in a

wide range of operating conditions cannot be characterized by a simple linear scaling of any one loading history.

A statistical model utilizing Monte Carlo numerical analysis methods has been presented to simulate service loading histories of a passenger vehicle. This model can measure and extrapolate Weibull curve-fitted cumulative exceedance diagrams to quantify the distribution of service loading histories. Also described was an automated curve fitting routine for the fitting of a single higher magnitude 3 parameter Weibull curve to any given set of exceedance data. The Monte Carlo obtained a distribution for service loading under a variety of service conditions by using data obtained from a novel approach of using a Four-Wheel Drive All Terrain Vehicle to model passenger vehicle service loading data. Overall, this statistical method of fatigue analysis described holds definite potential.

REFERENCES

1. Socie, D. F., and Park, K. "Analytical Descriptions of Service Loading Suitable for Fatigue Analysis" Proceedings of the Tenth International Conference on Vehicle Structural Mechanics and CAE, SAE P308, pp203-206, 1997

2. Socie, D. F., and S. D. Downing "Statistical Strain-Life Fatigue Analysis" SAE Paper 960566, 1996